

# Non-LTE line formation in clumpy and turbulent molecular clouds

M. Hegmann and W.H. Kegel

Institut für Theoretische Physik der Johann Wolfgang Goethe Universität Frankfurt, Robert-Mayer-Strasse 8–10,  
60054 Frankfurt am Main, Germany

Received 2 February 2000 / Accepted 4 May 2000

**Abstract.** Extending previous work (Albrecht & Kegel 1987, Kegel et al. 1993, Piehler & Kegel 1994), we investigated the formation of interstellar molecular lines in a medium with stochastic density and velocity fluctuations. We solved the full NLTE–problem, i.e. the generalized radiative transfer equation simultaneously with the rate equations, for a 6–level CO molecule and a plane-parallel slab geometry. Our results indicate that accounting for a finite correlation length of both, the density and velocity field, strongly affects the line profile and the line width as well as the intensity ratios of different rotational transitions.

**Key words:** line: formation – radiative transfer – ISM: clouds – ISM: molecules – radio lines: ISM

## 1. Introduction

Observations of molecular emission lines with high spatial resolution indicate that the cold and dense molecular medium has a tendency to be extremely inhomogeneous. Due to this observational evidence line formation in a clumpy medium was investigated by several authors (see e.g. Juvela 1996, Pagani 1997, Park & Hong 1995). Their studies are mainly based on Monte Carlo simulations assuming a model cloud consisting of a finite number of distinct phases (different particle densities).

We consider in this paper a concept that takes a continuous range of particle densities into account. Our work is mainly based on a theoretical approach which was developed by Gail and collaborators (Gail et al. 1974, Gail & Sedlmayr 1974a, Gail et al. 1975) in order to describe the formation of spectral lines in a turbulent velocity field with a finite correlation length. In a series of papers (Albrecht & Kegel 1987, Kegel et al. 1993, Piehler & Kegel 1994, paper I to III hereafter) we applied this theory to the formation of CO emission lines in the millimeter and submillimeter range. We could show that accounting for a finite correlation length strongly affects the line shapes, as well as the equivalent widths. It is the aim of the present paper to investigate the additional influence of an inhomogeneous, stochastic density distribution on the line formation process. In our model, both the velocity and the density distribution along the line of

sight are described by Langevin equations. Due to the stochastic nature of the underlying density and velocity fields the intensity as well as the molecular occupation numbers have to be considered as random variables. It can be shown that, under the above assumptions (see e.g. Gail et al. 1980), the ordinary radiation transfer equation has to be replaced by a multidimensional Fockker–Planck equation. In the case of NLTE one must solve transfer and rate equations self-consistently for each point in physical, velocity and density space.

To demonstrate the importance of taking an inhomogeneous stochastic density distribution into account we performed NLTE calculations for rotational transitions of CO. Due to the enormous numerical effort we restricted the investigation to a 6–level model molecule and a simple plane–parallel slab geometry.

## 2. Basic equations

### 2.1. Stochastic description of the velocity and density distribution

We consider the formation of spectral lines in an inhomogeneous molecular cloud accounting for velocity and density fluctuations. Apriori we make the assumption that both the turbulent velocity field and the density distribution can be described in terms of their stochastic properties. This means that we must specify the functional form of the multipoint probability distributions. Following Gail et al. (1974), Traving (1980), and Hegmann & Kegel (1996) we assume a Markovian structure for the velocity and density field along each line of sight. In this approximation only two-point correlations are accounted for. Further, it is convenient to transform the hydrogen density to a logarithmic scale:

$$\tilde{n}(s) \stackrel{\text{def}}{=} \ln \left( \frac{n_{\text{H}_2}(s)}{n_{\text{ref}}} \right), \quad (1)$$

with  $n_{\text{ref}}$  being the reference hydrogen density. The one-point distributions of  $v$  (the turbulent velocity component along the line of sight  $s$ ) and  $\tilde{n}$  are then considered to be Gaussian

$$W_v(v) = \frac{1}{\sqrt{2\pi}\sigma_v} \exp \left( \frac{-v^2}{2\sigma_v^2} \right) \quad (2)$$

$$W_n(\tilde{n}) = \frac{1}{\sqrt{2\pi}\sigma_n} \exp \left( \frac{-\tilde{n}^2}{2\sigma_n^2} \right) \quad (3)$$

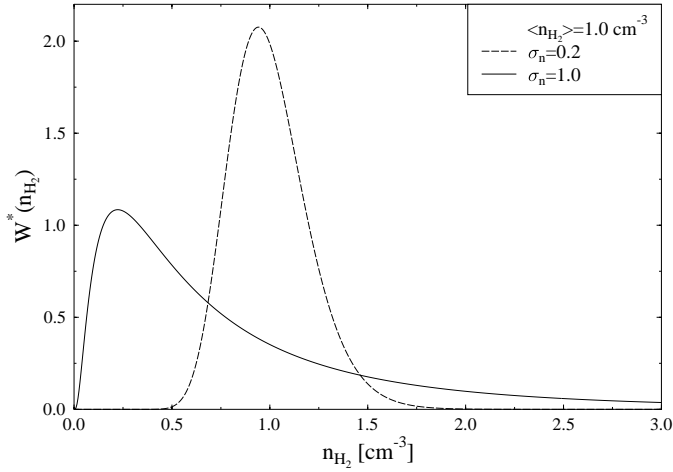


**Fig. 1.** One-point distribution function of the hydrogen number density

and the two-point correlation functions to be exponential

$$f_v(\Delta s) = \frac{\langle v(s)v(s+\Delta s) \rangle}{\sigma_v^2} = \exp\left(-\frac{|\Delta s|}{l_v}\right) \quad (4)$$

$$f_n(\Delta s) = \frac{\langle \tilde{n}(s)\tilde{n}(s+\Delta s) \rangle}{\sigma_n^2} = \exp\left(-\frac{|\Delta s|}{l_n}\right) \quad (5)$$

where  $l_v$  and  $l_n$  are the correlation lengths of the velocity and density field, respectively. Moreover, we neglect for our present study any correlations between the density and the velocity component  $v$ . This is an admissible lower order approximation, since only one velocity component, that along the line of sight, enters the transfer equation. Alternatively one can describe  $v(s)$  and  $\tilde{n}(s)$  along each line of sight by a set of Langevin equations (see Gail et al. 1974):

$$\frac{dv}{ds} = -\frac{v}{l_v} + \frac{\sigma_v}{\sqrt{l_v}}\Gamma_v(s) \quad (6)$$

$$\frac{d\tilde{n}}{ds} = -\frac{\tilde{n}}{l_n} + \frac{\sigma_n}{\sqrt{l_n}}\Gamma_n(s). \quad (7)$$

Here  $s$  is the spatial coordinate along the line of sight and  $\Gamma_n(s)$  and  $\Gamma_v(s)$  are the random noise or Langevin forces, which satisfy the following conditions:

$$\langle \Gamma_v(s) \rangle = 0, \langle \Gamma_v(s)\Gamma_v(s') \rangle = 2\delta(s-s') \quad (8)$$

and

$$\langle \Gamma_n(s) \rangle = 0, \langle \Gamma_n(s)\Gamma_n(s') \rangle = 2\delta(s-s'). \quad (9)$$

Eqs. (2) and (3) are, of course, solutions of (6) and (7).

## 2.2. About the structure of the density field

The two new model parameters  $\sigma_n$  and  $l_n$  have a simple physical meaning: The first quantity is a measure to which extent the mass of the cloud is concentrated in dense regions, whereas the latter is the length scale for the variation of the density. To illustrate this, we examine the distribution function of the real hydrogen number density. We insert Eq. (1) into (3) and obtain

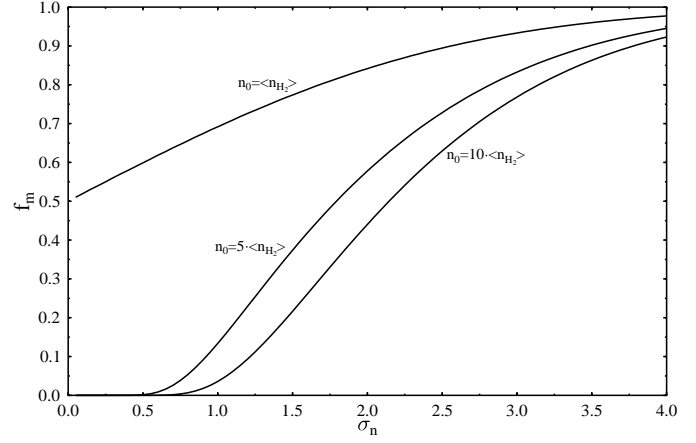


**Fig. 2.** Fraction of the mass contained in clumps denser than  $n_0$

$$\begin{aligned} W^*(n_{\text{H}_2})dn_{\text{H}_2} &= W(\tilde{n})d\tilde{n} \\ &= \frac{1}{n_{\text{H}_2}} \frac{1}{\sqrt{2\pi}\sigma_n} \exp\left(-\frac{1}{2\sigma_n^2} \left[\ln\left(\frac{n_{\text{H}_2}}{n_{\text{ref}}}\right)\right]^2\right) dn_{\text{H}_2}. \end{aligned} \quad (10)$$

From (10) the mean  $\langle n_{\text{H}_2} \rangle$  and the most probable density  $n_{\text{H}_2, \text{max}}$  can be calculated easily. It is:

$$\langle n_{\text{H}_2} \rangle = n_{\text{ref}} \cdot \exp\left(\frac{\sigma_n^2}{2}\right) \quad (11)$$

and

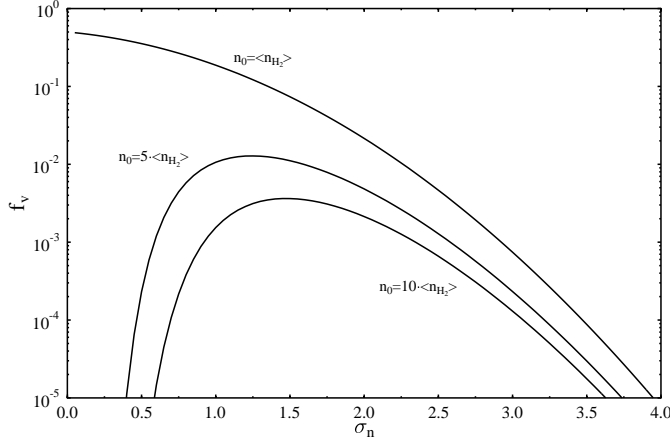
$$\begin{aligned} n_{\text{H}_2, \text{max}} &= n_{\text{ref}} \cdot \exp(-\sigma_n^2) \\ &= \langle n_{\text{H}_2} \rangle \cdot \exp\left(-\frac{3}{2}\sigma_n^2\right). \end{aligned} \quad (12)$$

Fig. 1 shows the distribution function of the hydrogen number density for two different values of the standard deviation of the logarithmic density distribution, but for the same mean hydrogen density. It can be clearly seen that for the higher value of  $\sigma_n$  the probability of finding a density, which is substantially smaller or greater than the mean density, is strongly increased. That is, for  $\sigma_n = 1.0$  most of the mass of our model cloud is concentrated in dense regions, which one may call clumps (cf. Fig. 4), whereas a low density gas fills most of the spatial volume of the cloud. To quantify these findings, we define two new functions  $f_m$  and  $f_v$ . The function  $f_m$  gives the fraction of the mass contained in parts of the cloud being denser than a lower limit  $n_0$  (see Fig. 2). It is given by

$$f_m(n_0, \sigma_n) = \frac{1}{\langle n_{\text{H}_2} \rangle} \int_{n_0}^{+\infty} n_{\text{H}_2} W_n^*(n_{\text{H}_2}) dn_{\text{H}_2}. \quad (13)$$

With increasing standard deviation of the logarithmic density distribution  $f_m$  approaches rapidly 1. We note in passing that for  $\sigma_n = 2.0$  almost 45% of the entire mass is contained in clumps being denser than  $10 \cdot \langle n_{\text{H}_2} \rangle$ . In contrast, the fraction of the volume  $f_v$  occupied by a gas denser than  $n_0$  strongly decreases with increasing  $\sigma_n$  (see Fig. 3). It is given by

$$f_v(n_0, \sigma_n) = \int_{n_0}^{+\infty} W_n^*(n_{\text{H}_2}) dn_{\text{H}_2}. \quad (14)$$



**Fig. 3.** Fraction of the volume occupied by a gas denser than  $n_0$

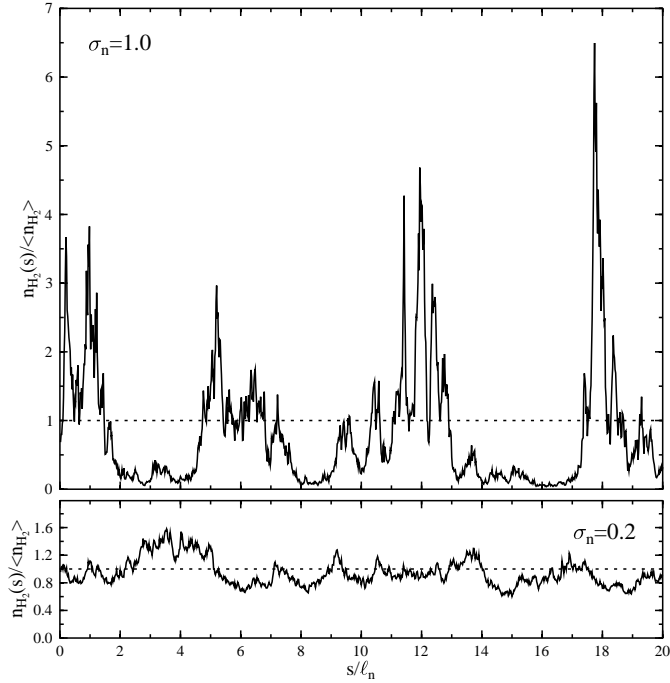


**Fig. 4.** Two concrete realizations of the stochastic density distribution given by Eq. (7) or Eqs. (3) and (5), respectively.

Although we are interested only in the expectation values of the relevant physical quantities, it may be very instructive to view single representations of the stochastic processes described above. Fig. 4 shows two concrete realizations of the density distribution  $n_{\text{H}_2}(s)$  along one line of sight. Though both distributions are smooth in principal, the distribution for  $\sigma_n = 1.0$  shows a clump like structure.

### 2.3. Generalized transfer and rate equations

It can be shown that for every set of Langevin equations, one can set up a Fockker-Planck equation by which the probability density of the stochastic variables can be calculated (see e.g. Risken 1988). The Langevin equations describing the stochastic

density and velocity field together with the ordinary radiation transfer equation, which can be formally written as

$$\frac{dI_\nu}{ds} = -\kappa_\nu (I_\nu - S_\nu) + 0 \cdot \Gamma_I(s), \quad (15)$$

lead to a multidimensional Fockker-Planck equation for the conditional intensity  $q_{\nu,s}(v, \tilde{n}, s)$  (Gail et al. 1974):

$$\begin{aligned} \frac{\partial q_{\nu,s}}{\partial s} = & \frac{1}{\ell_n} \left( -\tilde{n} \frac{\partial q_{\nu,s}}{\partial \tilde{n}} + \sigma_n^2 \frac{\partial^2 q_{\nu,s}}{\partial \tilde{n}^2} \right) + \frac{1}{\ell_v} \frac{\partial}{\partial v} \\ & \times \left( -v \frac{\partial q_{\nu,s}}{\partial v} + \sigma_v^2 \frac{\partial^2 q_{\nu,s}}{\partial v^2} \right) - \kappa_\nu (q_{\nu,s} - S_\nu). \end{aligned} \quad (16)$$

Eq. (16) is a partial differential equation with three independent variables  $s$ ,  $\tilde{n}$  and  $v$ , and has to be solved for a fixed frequency  $\nu$ . The expectation value of the intensity can be obtained from  $q_{\nu,s}(v, \tilde{n}, s)$  by a simple quadrature:

$$\langle I_\nu(s) \rangle = \int_{-\infty}^{+\infty} q_{\nu,s}(\tilde{n}, v, s) W_v(v) W_n(\tilde{n}) d\tilde{n} dv. \quad (17)$$

The source function  $S_\nu(v, \tilde{n}, s)$  and the absorption coefficient  $\kappa_\nu(v, \tilde{n}, s)$  are given in the usual way by the occupation numbers  $n_i$  and  $n_j$  of the level  $i$  and  $j$  corresponding to the transition considered, with

$$\kappa_\nu(v, \tilde{n}, s) = \kappa_\nu^0(v, \tilde{n}, s) \cdot \Phi_{ij}(\Delta\nu, v). \quad (18)$$

$\Phi_{ij}(\Delta\nu, v)$  is the normalized profile of the *local* absorption coefficient under the assumption of complete redistribution over this local profile. In view of the low densities prevailing in interstellar clouds we consider Doppler broadening to be the only broadening mechanism. That is,  $\Phi_{ij}(\Delta\nu, v)$  is given by

$$\begin{aligned} \Phi_{ij}(\Delta\nu, v) = & \frac{1}{\Delta\nu_{\text{therm}} \sqrt{\pi}} \\ & \times \exp \left( - \left( \frac{\Delta\nu}{\Delta\nu_{\text{therm}}} - \frac{v}{c} \frac{\nu_0}{\Delta\nu_{\text{therm}}} \right)^2 \right), \end{aligned} \quad (19)$$

with  $\nu_0$  being the frequency in the line center and  $\nu_{\text{therm}}$  being the thermal Doppler width.

In the case of NLTE the generalized transfer equation (16) has to be solved simultaneously with the system of rate equations for each point in coordinate, velocity and density space (see Gail et al. 1975):

$$\begin{aligned} & \sum_{j \neq i} [n_j (A_{ij} + C_{ij}) - n_i (A_{ji} + C_{ji})] \\ & + \sum_{j \neq i} (n_j B_{ij} - n_i B_{ji}) \frac{4\pi}{c} \langle \Phi_{ij} q_{\nu,s} \rangle = 0. \end{aligned} \quad (20)$$

It has to be noted that now the occupation numbers not only depend on the spatial coordinate but also on the velocity and the logarithmic density.  $\langle \Phi_{ij} q_{\nu,s} \rangle$  is the mean and angle averaged value of the local radiation field, weighted with the profile function of the local absorption coefficient, which depends on  $v$  and  $\tilde{n}$ , too. We approximate it by (see paper I):

$$\langle \Phi_{ij} q_{\nu,s} \rangle = \frac{1}{4\pi} \int_0^\infty \int_\Omega \Phi_{ij}(\Delta\nu, v) q_{\nu,s}(v, \tilde{n}, s) d\Omega dv. \quad (21)$$

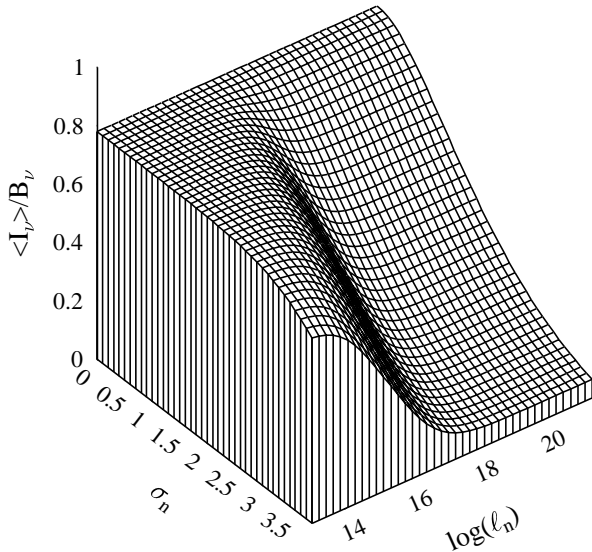


**Fig. 5.** LTE expectation values of the intensity in the center of the  $J = 2 \rightarrow 1$  line for  $\langle N_{\text{CO}} \rangle = 1.6 \cdot 10^{16} \text{cm}^{-2}$ ,  $\langle n_{\text{H}_2} \rangle = 10^3 \text{cm}^{-3}$  and a microturbulent velocity field with  $\sigma_v/v_{\text{th}} = 10$ .

The  $A_{ij}$  and  $B_{ij}$  are the Einstein coefficients for spontaneous and induced transitions, while the  $C_{ij}$  denote the probability for collisional transitions  $j \rightarrow i$ . For calculating the radiative transition rate, we set the dipole moments of the CO-molecule to 0.112 Debye (Spitzer 1988), and for the CO-H<sub>2</sub> collisions we used rate coefficients given by Flower & Launay (1985).

It should be noted in passing that the generalized transfer equation (16) implies an incomplete redistribution of photons over the line profile. In writing (16) we assume complete redistribution only over the local thermal profile, whereas the redistribution caused by the turbulent velocity field is partial. Consequently, the occupation numbers have to depend on the turbulent velocity. This is in contrast to the usual microturbulent approach, where complete redistribution is assumed over a profile, which includes the broadening by the turbulent velocity.

### 3. Results

Our calculations are based on Eqs. (16), (20) and (21). The numerical techniques we used are essentially the same as discussed in paper I and II. As before, we study the formation of CO rotational lines in an on average homogeneous plane parallel slab, which is illuminated from both sides by the cosmic background radiation. Thus, we have independently of the velocity and density for  $s = 0$  the initial condition

$$q_{\nu,s}(v, \tilde{n}, s) = I_{\nu,0} = B_\nu(2.7 \text{ K}). \quad (22)$$

For a typical dark cloud, we assume a kinetic gas temperature of  $T_{\text{gas}} = 10 \text{ K}$  and average H<sub>2</sub> number densities between  $n_{\text{H}_2} = 10^3 \text{cm}^{-3}$  and  $n_{\text{H}_2} = 10^4 \text{cm}^{-3}$ . The relative CO abundance is considered to be constant throughout the cloud. We adopted the value given by Black & Willner (1984), i.e.  $n_{\text{CO}}/n_{\text{H}_2} = 8 \cdot 10^{-5}$ . The CO molecule was approximated by a rigid rotor with 6 energy levels.

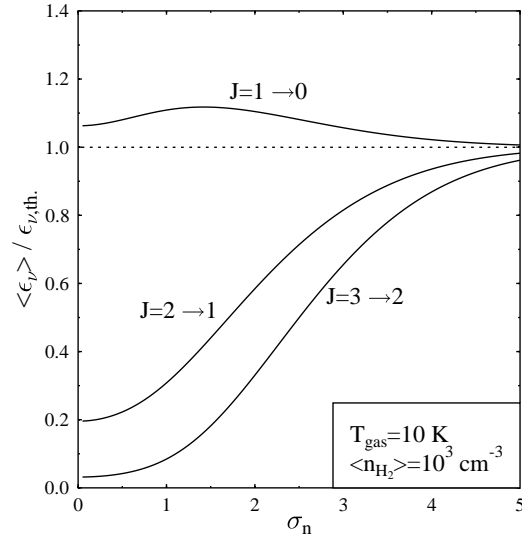


**Fig. 6.** Emission coefficients for rotational transitions of CO in the case of optically thin lines and a 3K-background. All values are normalized to their corresponding thermal values.

#### 3.1. Microturbulence

Our objective is mainly to investigate how an inhomogeneous, stochastic density distribution affects the line formation process. Hence, we consider first of all a simple microturbulent velocity field excluding all effects due to a finite correlation length of the turbulent velocity field. Consequently, the generalized radiative transfer equation (16) reduces to

$$\frac{\partial q_{\nu,s}}{\partial s} = \frac{1}{\ell_n} \left( -\tilde{n} \frac{\partial q_{\nu,s}}{\partial \tilde{n}} + \sigma_n^2 \frac{\partial^2 q_{\nu,s}}{\partial \tilde{n}^2} \right) - \kappa_\nu (q_{\nu,s} - S_\nu). \quad (23)$$

From these calculations one can see, that the density fluctuations act upon the process of line formation essentially by two mechanisms. On the one hand, radiative transfer itself is affected. Fig. 5 shows the LTE expectation value of the intensity  $\langle I_\nu \rangle$  in the center of the  $J = 2 \rightarrow 1$  line as function of the standard deviation of the logarithmic density  $\sigma_n$  and the correlation length of the density field  $\ell_n$ , respectively. The adopted average column density is  $\langle N_{\text{CO}} \rangle = 1.6 \cdot 10^{16} \text{cm}^{-2}$ . It can be clearly seen that the mean intensity decreases with both, an increasing  $\sigma_n$  and an increasing  $\ell_n$ . These findings are plausible: In the case of a high standard deviation of the logarithmic density most of the mass of the cloud is concentrated in very dense and spatially small regions, whereas most of the spatial volume is filled with a gas of rather low density. The extension of these dense regions and the mean distance between them scale with the correlation length  $\ell_n$ . Due to this dilution effect the mean intensity can be substantially smaller than the corresponding value obtained for a homogeneous cloud with the same mean H<sub>2</sub> number density. The effect becomes pronounced for  $\kappa_\nu^0 \ell_n \gtrsim 1$ .

On the other hand, the density fluctuations act directly upon the occupation numbers of the molecule. Since the rate of collisional transitions depends on the square of the hydrogen density, the mean rate of transitions due to CO-H<sub>2</sub> collisions does not

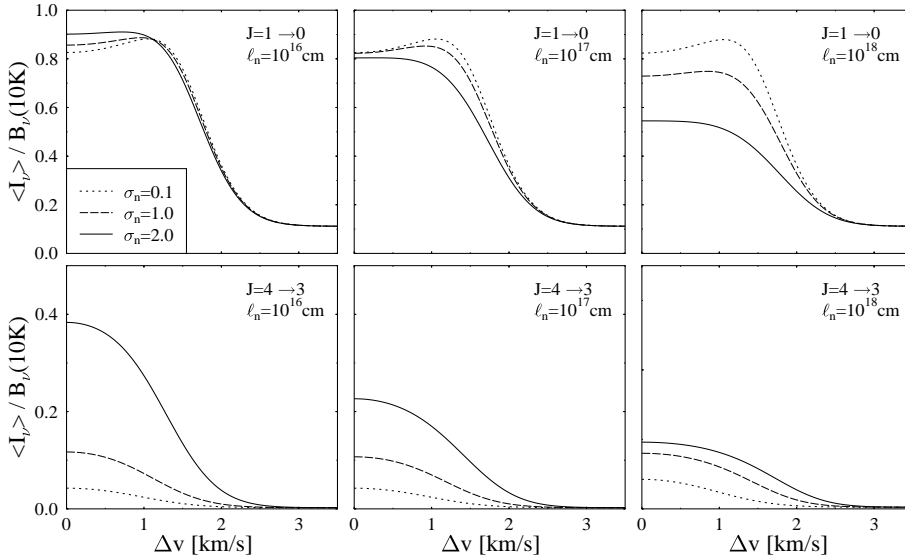


**Fig. 7.** Line profiles for rotational transitions  $J = J + 1 \rightarrow J$  of CO for  $T_{\text{gas}} = 10$  K,  $\langle n_{\text{H}_2} \rangle = 10^3 \text{ cm}^{-3}$ ,  $\langle N_{\text{CO}} \rangle = 10^{17} \text{ cm}^{-2}$  and a microturbulent velocity field with  $\sigma_v/v_{\text{th}} = 10$ .

only depend on the first moment of the logarithmic density distribution, but also on its second moment  $\sigma_n^2$ . To exclude effects due to radiative transfer we show in Fig. 6 the expectation value of the emissivity  $\langle \epsilon_\nu \rangle$  for the three lowest rotational transitions of CO in the optically thin limit. As an external radiation field we again assume only the 3K-background radiation. It can be clearly seen that for a high standard deviation  $\sigma_n$  the emission coefficient approximates the corresponding LTE value rather well. This result can be explained easily: As for large values of  $\sigma_n$  most of the mass of our model cloud is concentrated in very dense clumps, collisional transitions dominate the corresponding radiative transitions. The occupation numbers thermalize, i.e. they are given by a Boltzmann distribution.

Fig. 7 gives line profiles for the  $J = 1 \rightarrow 0$  and  $J = 4 \rightarrow 3$  transitions of CO. (In Figs. 7, 9 and 10 we use the usual convention to describe the line profile by the Doppler shift  $\Delta v$  which corresponds to  $\Delta\nu = \nu - \nu_0$  in Eq. (16).) The adopted average column density is  $\langle N_{\text{CO}} \rangle = 10^{17} \text{ cm}^{-2}$ . The different profiles within one frame correspond to different standard deviations of the logarithmic density, whereas from one frame to the other the correlation length of the density field is altered. The two effects discussed above are clearly seen. The line intensities of the  $J = 1 \rightarrow 0$  transition, which thermalizes at rather low densities, is noticeably decreased for large values of  $\sigma_n$  and  $\ell_n$ . The intensity of the  $J = 4 \rightarrow 3$  transition, on the other hand, increases substantially with increasing  $\sigma_n$ . In this case, radiation is basically emitted from dense clumps, where the high rotational levels can be populated efficiently by collisions of CO with  $\text{H}_2$ . But again, the intensity decreases with increasing correlation length. In addition to the line profiles, in Fig. 8 the ratio of the  $J = 4 \rightarrow 3$  to the  $J = 1 \rightarrow 0$  intensities in the line center is given as function of  $\ell_n$ , normalized to the respective values of the Kirchhoff-Planck function.

Another point of interest is the weak self-absorption in the center of some of the  $J = 1 \rightarrow 0$  lines. This feature, which gets even more dominant for high optical depths, is due to NLTE and optical thickness effects. As the escape probability of photons

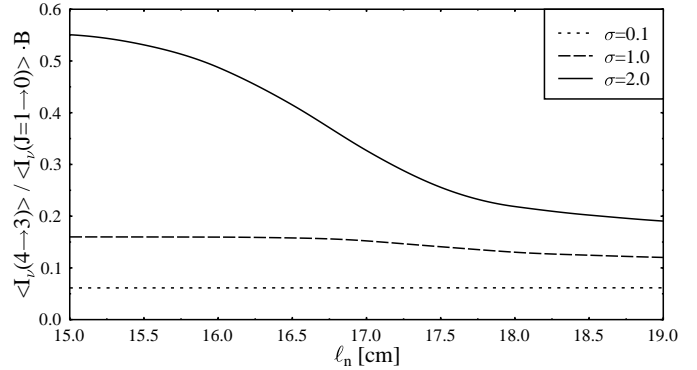


**Fig. 8.** Ratio of the  $J = 4 \rightarrow 3$  to  $J = 1 \rightarrow 0$  intensities in the line center, normalized to the respective values of the Kirchhoff-Planck function. In our particular case,  $T_{\text{gas}} = 10$  K,  $B$  is given by:  $B = B_{115}(10K)/B_{460}(10K) \approx 0.173$ . The calculations were performed for  $T_{\text{gas}} = 10$  K,  $\langle n_{\text{H}_2} \rangle = 10^3 \text{ cm}^{-3}$ ,  $\langle N_{\text{CO}} \rangle = 10^{17} \text{ cm}^{-2}$  and a microturbulent velocity field with  $\sigma_v/v_{\text{th}} = 10$ .

becomes smaller towards the center of the cloud, a gradient in the excitation temperature with cloud depth builds up. Then, in the line center, where the optical depth is large, we see radiation from the outer part of the cloud, whereas in the wings the contribution from regions deep within our model cloud dominates.

### 3.2. Turbulent velocity field with finite correlation length

Indeed, it is a well known problem of microturbulent velocity models to predict deep self-absorption features which are rather rarely observed in molecular spectra. As has been shown before (see especially paper II) self-absorption is strongly reduced, if one accounts for a finite correlation length of the turbulent velocity field. In writing the generalized radiative transfer equation (16), we adopted the same velocity model.

Figs. 9 and 10 give line profiles for the  $J = 1 \rightarrow 0$  and  $J = 4 \rightarrow 3$  transitions of CO which have been calculated for a mesoturbulent velocity field. The adopted average column

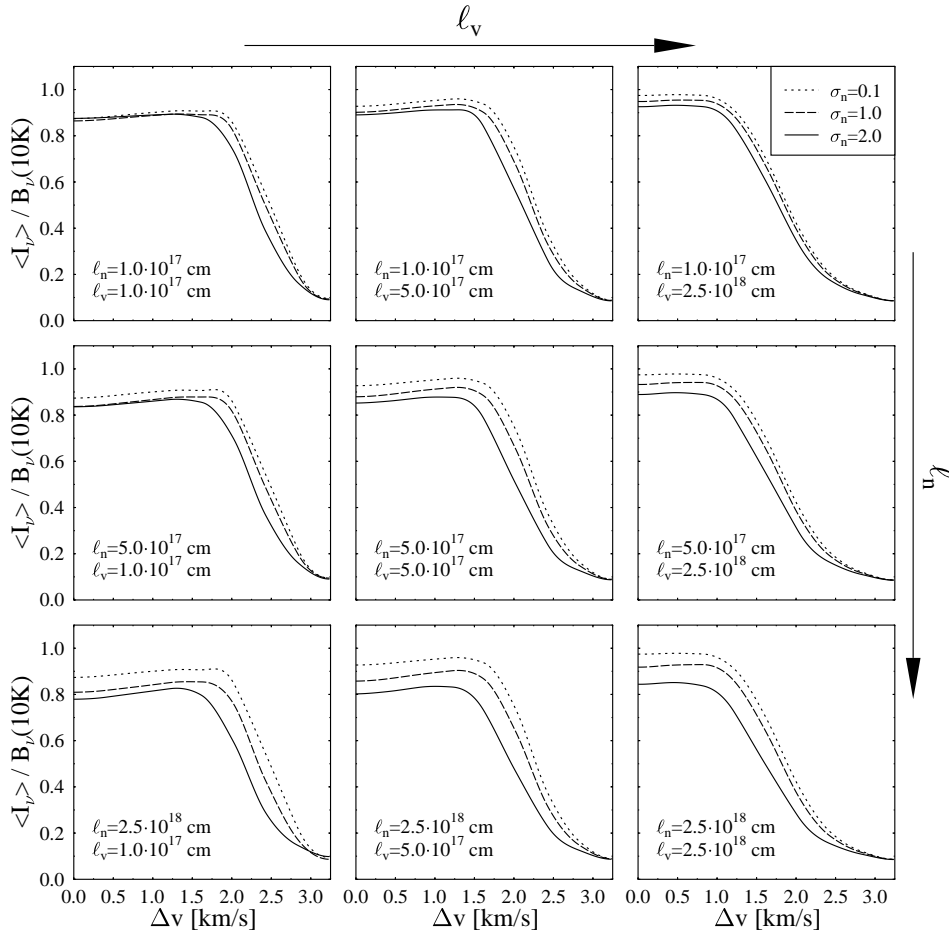


**Fig. 9.** Line profiles for the  $J = 1 \rightarrow 0$  transition of CO for  $T_{\text{gas}} = 10$  K,  $\langle n_{\text{H}_2} \rangle = 10^3 \text{cm}^{-3}$ ,  $\langle N_{\text{CO}} \rangle = 2.4 \cdot 10^{18} \text{cm}^{-2}$  and  $\sigma_v/v_{\text{th}} = 10$ .

density is  $\langle N_{\text{CO}} \rangle = 2.4 \cdot 10^{18} \text{cm}^{-2}$ . Again, the different profiles within one frame correspond to different standard deviations of the logarithmic density, while from one frame to the other the correlation lengths of the velocity and density field are varied. As to be expected from the results discussed in Sect. 3.1, the  $J = 4 \rightarrow 3$  lines are substantially increasing with higher values of  $\sigma_n$ . In contrast, the  $J = 1 \rightarrow 0$  lines become slightly weaker with increasing  $\sigma_n$ . Beyond that, it can be seen that for the nearly homogeneous density distribution  $\sigma_n = 0.1$  the intensity in the line center increases with increasing correlation length of the velocity field. This finding is not that surprising, as the mean free path of the photons is a function of  $\ell_v$ . If we consider only one line of sight, i.e. if we consider  $q_{\nu,s}$  instead of the mean intensity  $\langle I_\nu \rangle$ , we find that the line width decreases with increasing  $\ell_v$ . In the limit  $\ell_v \rightarrow \infty$ , the line width corresponds actually to that in the case of purely thermal line broadening. Hence, saturation effects set in at smaller values of the column density. For high values of  $\sigma_n$ , this effect becomes less important. The occupation numbers of the molecule then are dominated by collisions and, consequently, NLTE effects become insignificant.

In addition to the line profiles, in Fig. 11 the curves of growth for the four lowest rotational transition of CO are shown. Here, we plotted for a fixed set of correlation lengths  $\ell_n = \ell_v = 5 \cdot 10^{17} \text{cm}$  the mean equivalent width

$$\langle W_\lambda \rangle = \int_{\text{line}} \frac{\langle I_\lambda \rangle - B_\lambda(2.7 \text{ K})}{B_\lambda(2.7 \text{ K})} d\lambda, \quad (24)$$

with  $\lambda_0$  being the wavelength in the line center, against the mean column density of CO.

Besides the mechanisms discussed above, another NLTE and optical thickness effect can be seen clearly in Fig. 11: For the  $J = 3 \rightarrow 2$  and  $J = 4 \rightarrow 3$  lines and  $\sigma_n = 2.0$ , the curves of growth steepen with increasing  $\langle N_{\text{CO}} \rangle$  over a sensitive range of CO column densities. Moreover, for the  $J = 4 \rightarrow 3$  line and  $\sigma_n = 0.1$  the slope of the curve of growth becomes even larger than unity in the log-log-plot. In order to understand this result, one has to take the process of photon trapping into account. With increasing optical depth, the escape probability of photons decreases and, consequently, the local excitation temperature increases towards its LTE value in the inner parts of the cloud.

#### 4. Conclusions

In the preceding Sects. we discussed the formation of interstellar molecular lines in a clumpy and turbulent medium. In particular, we focused our efforts on determining the effects caused by an inhomogeneous stochastic density distribution. To this end, we assumed a 6-level model molecule and a plane-parallel slab geometry. It turned out that especially high rotational transitions are affected.

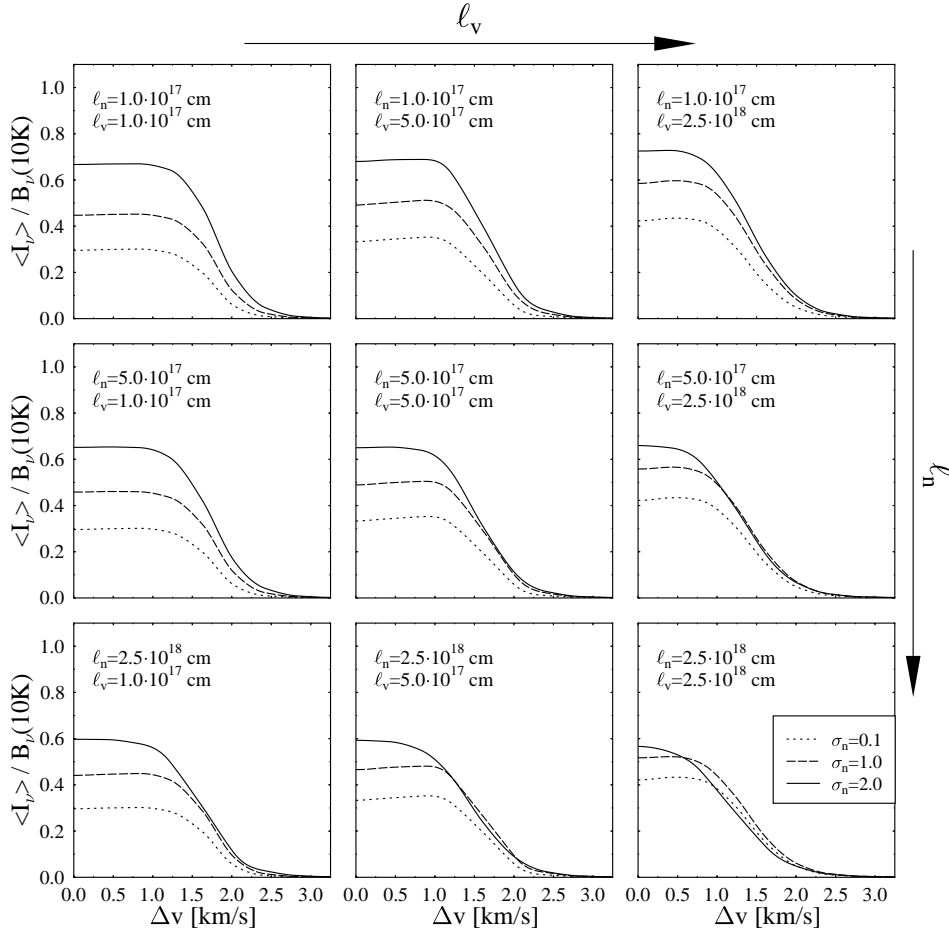


**Fig. 10.** Line profiles for the  $J = 4 \rightarrow 3$  transition of CO for  $T_{\text{gas}} = 10$  K,  $\langle n_{\text{H}_2} \rangle = 10^3 \text{cm}^{-3}$ ,  $\langle N_{\text{CO}} \rangle = 2.4 \cdot 10^{18} \text{cm}^{-2}$  and  $\sigma_v/v_{\text{th}} = 10$ .

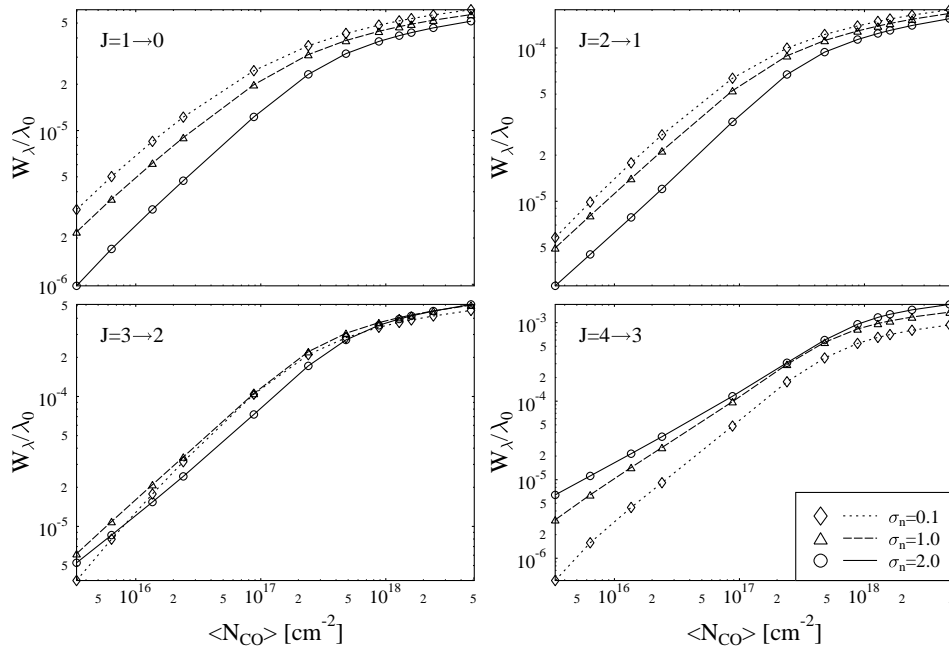


**Fig. 11.** Curves of growth for the four lowest rotational transitions of CO for  $T_{\text{gas}} = 10$  K,  $\langle n_{\text{H}_2} \rangle = 10^3 \text{cm}^{-3}$  and  $\sigma_v/v_{\text{th}} = 10$ .

The results can be summarized as follows: Lines of low rotational transitions become in most cases weaker with an increasing value of the standard deviation of the logarithmic density distribution. In contrast, high rotational lines tend to be substan-

tially stronger than is consistent with a uniform density model. By accounting for a finite correlation length of the mesoturbulent velocity field self-absorption is considerably reduced, and lines look saturated although the LTE limit is not reached.

These effects demonstrate that physical parameters of molecular clouds derived by a classical analysis (i.e. micro-turbulent velocity field, complete redistribution of photons over the whole line profile and a homogeneous density distribution) of observational data may have to be corrected.

*Acknowledgements.* We wish to thank our referee E. Falgarone whose comments and recommendations significantly improved the paper. This work was supported in part by the German Bundesministerium für Bildung, Wissenschaft, Forschung und Technologie (BMBF) in the frame of the project No 053FM13A.

## References

- Albrecht M.A., Kegel W.H., 1987, A&A 176, 317  
Black J.H., Willner S.P., 1984, ApJ 279, 673  
Flower D.R., Launay J.M., 1985, MNRAS 214, 271  
Gail H.P., Hundt E., Kegel W.H., et al., 1974, A&A 32, 65  
Gail H.P., Sedlmayr E., 1974a, A&A 36, 17  
Gail H.P., Sedlmayr E., Traving G., 1975, A&A 44, 421  
Gail H.P., Sedlmayr E., Traving G., 1980, J. Quant. Spectr. Radiat. Transfer 23, 267  
Hegmann M., Kegel W.H., 1996, MNRAS 283, 167  
Juvela M., 1996, A&A 322, 943  
Kegel W.H., Pihler G., Albrecht M.A., 1993, A&A 270, 407  
Pagani L., 1997, A&A 333, 269  
Park Y.-S., Hong S.S., 1995, A&A 300, 890  
Pihler G., Kegel W.H., 1994, A&A 297, 841  
Risken H., 1988, The Fokker–Planck Equation. Berlin Heidelberg: Springer  
Spitzer L., 1978, Physical Processes in the Interstellar Medium. New York: Wiley-Interscience  
Traving G., 1980, A&A 85, 281